Journal of Structural Geology, Vol. 14, No. 8/9, pp. 981 to 990, 1992
Printed in Great Britain

0191-8141/92 $05.00+0.00

Comparison between connected and overall porosity of thermally stressed granites

YVES GÉRAUD

Laboratoire de Géologie Structurale et Appliquée, Université de Provence, 3 Place Victor Hugo, case 28, F-13331 Marseille Cédex 3, France and GLM/CNRS/LMA/MESH, 31 chemin J. Aiguier, F-13274 Marseille Cédex 9, France

F. MAZEROLLE

GLM/CNRS/LMA/MESH, 31 chemin J. Aiguier, F-13274 Marseille Cédex 9, France

and

SUZANNE RAYNAUD

Laboratoire de Géologie Structurale et Appliquée, Université de Provence, 3 Place Victor Hugo, case 28, F-13331 Marseille Cédex 3, France

(*Received* 3 *October* 1991; *accepted in revised form* 29 *April* 1992)

Abstract—The structural evolution of four granites, heated from 20 to 700°C, was examined after cooling. The granites have four typical initial structures, which can be sub-divided into two groups: rocks with high connected porosity; comprising cracks with low aspect ratio and alteration pores (type A), pores and a few cracks (type B), or cracks (type C); and rocks with low connected porosity, with cracks (type D).

The connected porosity was measured by mercury injection, and the total porosity by X-ray computerized tomography. At low temperature ($T < 300$°C), the connected porosity decreases with increasing temperature, particularly for the material with high crack density and connected porosity (A and B). The total porosity increases for B, C and D, and decreases for the material with low aspect ratio cracks (A). Above 300°C, both porosities increase. The data show that the thermal history of a granite can be decomposed into two phases. In the first stage the connected porosity decreases with increasing temperature, cracks are initiated at low temperature and they form unconnected networks. In the second stage, the connected and total porosities increase, the previously initiated cracks form a connected network by opening, and they interact with newly created cracks.

INTRODUCTION

MANY situations such as geothermal energy or disposal of nuclear waste involve the heating and cooling of rocks, particularly granitic rocks.

In polycrystalline rocks thermal cracking originates from local stress concentrations induced by anisotropic dilatation and/or variations in thermal expansion (Friedman & Johnson 1978). Thermally induced cracks have a great influence on the mechanical and permeability properties of the rock. A review of the various petrophysical characteristics of thermally deformed rocks has been given by Heuze (1983). Thermal crack formation can influence the local stress state at different depths, the transport phenomena in hydrothermal systems in crystalline rocks, and the formation of porous networks in crustal rocks (Norton & Knight 1977). Microstructural studies of rocks, especially of the distribution of apertures, has been frequently done using SEM observations which show that the porous network is heterogenous (Fig. 1).

The porosity of unheated granites is composed mainly of cracks, for unweathered and stressed material (Sprunt & Brace 1974, Krantz 1980, 1983). Pores occur when weathering phenomena have occurred, generally after crack formation and fluid circulation (Sprunt & Brace 1974, Norton & Knapp 1977). During thermal testing, the initial crack density is an important parameter, and certain values can result at low temperatures in a decreasing dilatancy of the rock (Cooper & Simmons 1977). At higher temperatures, the initial cracks can act as sites for the nucleation of thermal cracks (Friedrich & Wong 1986, Wang *et al.* 1989).

In this paper we want to show how the type and amount of porosity are important factors controlling thermal cracking. To study thermal cracking, four granites with different porous structures were chosen. The samples were characteristic of nonweathering, a low degree of weathering, a high degree of weathering or a mechanically stressed granitic structure. Samples were heated to different temperatures and cooled (rates less than 50°C h^{-1}), then the porosity was characterized by different techniques which gave us data on the porosity distribution. Connected porosity values and throat size of the network (see section on "Mercury injection porosity") were determined by mercury injection. Total

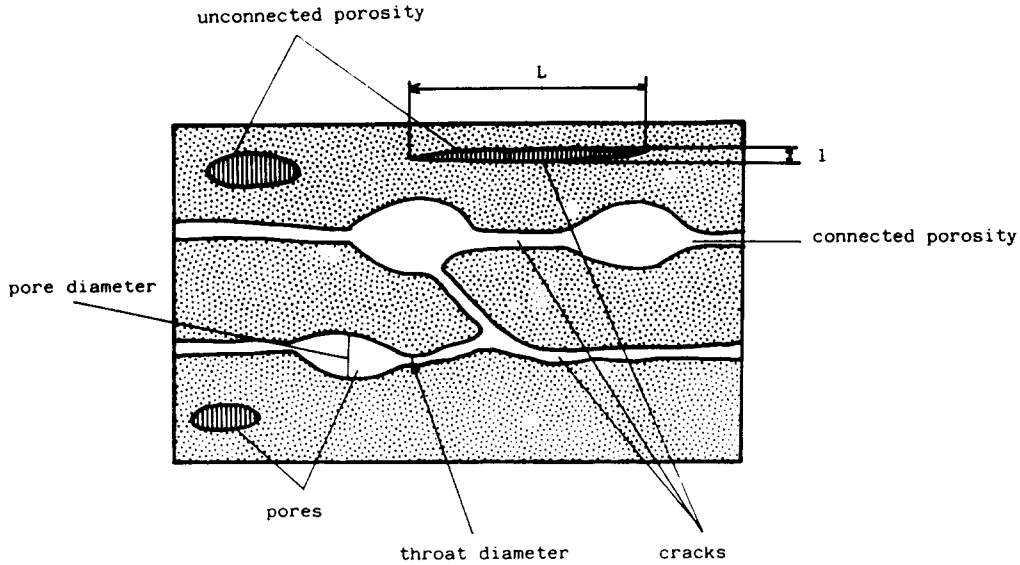

Fig. 1. Porosity model for granitic rocks. The porosity is composed of two types of microstructures : pores and cracks. They are distinguished by their aspect ratio (l/L ratio). A pore aspect ratio is defined as less than 10^{-1}, and a crack aspect ratio as more than 10^{-1}. This structure comprises the total porosity, which is divided into connected porosity and unconnected porosity. Throat diameter is the parameter depending on the pressure injection for mercury porosimetry and can be related to the crack width. The ratio throat diameter/pore diameter is the first parameter which induces trapped porosity.

porosity (connected porosity + unconnected porosity) was calculated from the radiological density obtained by X-ray computerized tomography (CT). SEM observations provide semi-quantitative values of total porosity and data on the type of discontinuities which constitute the porosity. These measurements were undertaken on four granites with different porous networks and grain size in order to compare the influence of these initial parameters on the modification of the porous networks after thermal treatment.

MEASUREMENT PROCEDURES

Three techniques were used to measure porosity and determine the corresponding structures. Connected porosity was measured by mercury injection, total porosity by computer tomography (CT) and microstructures were determined by observation of polished sections in the SEM. Thus aperture geometry, volume, size, pore and crack type (open or closed) could be determined (Fig. 1).

For each type of granite, samples from different locations were heated at various temperature and then cooled. In each location three cores (14 mm in diameter, 25 mm of length) were tested by mercury injection and another three samples were cored and mechanically polished for the SEM observations. CT measurements were made on the same sample at room temperature, after being heated to the indicated maximum temperature and cooled. For all samples, each heating–cooling cycle was conducted at a temperature stepping rate of less than 50°C h^{-1}. The indicated maximum temperature was maintained for 20 h.

Mercury injection porosity measurements

This technique consists of measuring the volume of mercury injected into a previously dessicated, degasified sample for different steps of increasing values of mercury pressure. Each mercury pressure depends on the throat diameter by the Washburn relationship (Washburn 1921)

$$P = 2\gamma \cos \theta / D \quad (1)$$

for a tube structure (D is a tube diameter) and by the Lenormand relationship (Lenormand *et al.* 1983)

$$P = 2\gamma \cos \theta / x \quad (2)$$

for a rectangular section structure (x is the smallest dimension of the section, for cracks), where P is the pressure measured in mercury, γ is air–mercury interfacial tension, θ is the constant angle measured in mercury. D and x values are alternative terms for throat diameter.

For each pressure step, the porosity volume is dependant on the throat diameter, which is the smallest characteristic of the void geometry. For the granitic microstructure, the throat diameter can be compared with crack width.

Three different characteristics of the connected porous network can be determined: (a) the connected porosity; (b) the trapped porosity; and (c) the porosity spectrum.

The connected porosity value is given by the volume of injected mercury at the maximum pressure (150 MPa). Each value corresponds to the average porosity from three samples.

The trapped porosity is the mercury volume which is not expelled from the sample when the pressure is

Table 1. Petrographic parameters for granites A, B, C and D

	A	B	C	D
Grain size (mm)	1–5	0.1–0.5	0.5–2	1–5
Roughness	high	low	high	low
Porosity (%)	1.77	2.3	1.5	0.48
Pore size (μm)	<2	0.1–0.3	<2	0.01–0.03 0.1–0.4
Trapped porosity (%)	70	80	36	67
Discontinuities	pore crack	pore canal cracks	cracks pore	cracks pore

released. The value of the trapped porosity is comparable to the pore volume of the rock (Li & Wardlaw 1986). This value depends on the ratio of pore diameter to throat diameter. There is a critical value above which mercury is trapped. Wardlaw *et al.* (1988) found critical values from 1.6 to 2.0 for dolomite, for example.

Porosity spectrum is the measurement of the connected porosity at each pressure step or throat diameter step (cf. Washburn or Lenormand equations, 1 and 2). This curve is a cumulative curve and is termed the porosity spectrum. These data can be interpreted using percolation theory to give us the absolute permeability; the calculated values involve no adjustable parameters. Katz & Thompson (1987) defined the inflection point of the cumulative injection curve as the point at which the mercury first forms a continuous cluster across the sample. The results obtained by Guegen & Diennes (1989) from percolation theory show that, for a crack population, the permeability depends on the throat diameter and the porosity value, where these parameters could be determined by mercury porosimetry.

X-ray computerized tomography

This technique was originally used for medical purposes, before being adapted to observe rocks (Raynaud *et al.* 1989). It is based on measuring the attenuation of X-ray beams and defines a radiological density. These data are influenced by the chemical composition and the total porosity of the sample. CT is a non-destructive technique, so that radiological density can be measured on the same sample after several different thermal cycles.

The variations in gravimetric density and thus in overall porosity can be calculated from the mean radiological density at different stages of deformation. Porosity variations in the sample set are given by the formula (Géraud *et al.* 1991):

$$\Delta n = \Delta H/300 d_0, \quad (3)$$

where Δn is the porosity variation, ΔH is the radiological density variation and d_0 is the initial value of gravimetric density. For each sample a set of 11 2-mm sections was carried out in the same zone in the initial state and then again after each heating cycle. By averaging the density of each section the porosity evolution over a large volume of the sample could be followed.

Each section corresponded to 1.9 cm^3, thus giving an analysis volume of 20.9 cm^3 for the 11 sections.

SEM observations

This technique provides some insight into the type of discontinuity, and semi-quantative data on the relative importance of these discontinuities. The approach has been used previously to describe thermally induced deformations, but here it is specifically used to corroborate the results given by mercury injection porosity measurements and CT.

The method for quantification of discontinuities is taken from Tapponier & Brace (1976). Five pictures of each granite (A, B and D samples) at 20°C and after the heating–cooling cycle were analysed. On each photograph eight scanlines were drawn and each void crossed by one of these lines was counted and classified in terms of its smallest dimension and its type (pore or crack, where the boundary between them is at aspect ratio $\alpha = 1/10$).

DESCRIPTION OF MATERIAL

Four calc-alkaline granites were chosen for their different porous networks. Their modal compositions determined by counting 2000 points on four thin sections are shown in Table 1. The weathering of the different mineral phases is also shown as it is an important factor in the amount and kind of porosity. The greater the weathering, the higher the porosity and the pore density, except in certain conditions of fluid circulations where the rate of weathering is inversely proportional to the connected porosity in the material (Katsube & Kaminemi 1983). The data in Table 2 deal with structural parameters of the samples including grain size, connected porosity volume and type of discontinuities in the rock.

Table 2. Structural parameters for granites A, B, C and D

	A	B	C	D
Quartz	26.8	37.1	34.6	33.7
Feld. pl.	33.6	25.6	34.9	35.4
Feld. K	26.3	31.9	18	19.4
Biotite	13	1.2	6.7	8.3
Muscovite		4.2	5.8	3
Hornblende	0.4			
Weathering feld. pl.	moderate	high	low	high
Feld. K	high	moderate	low	low
Biotite	high	moderate	low	high

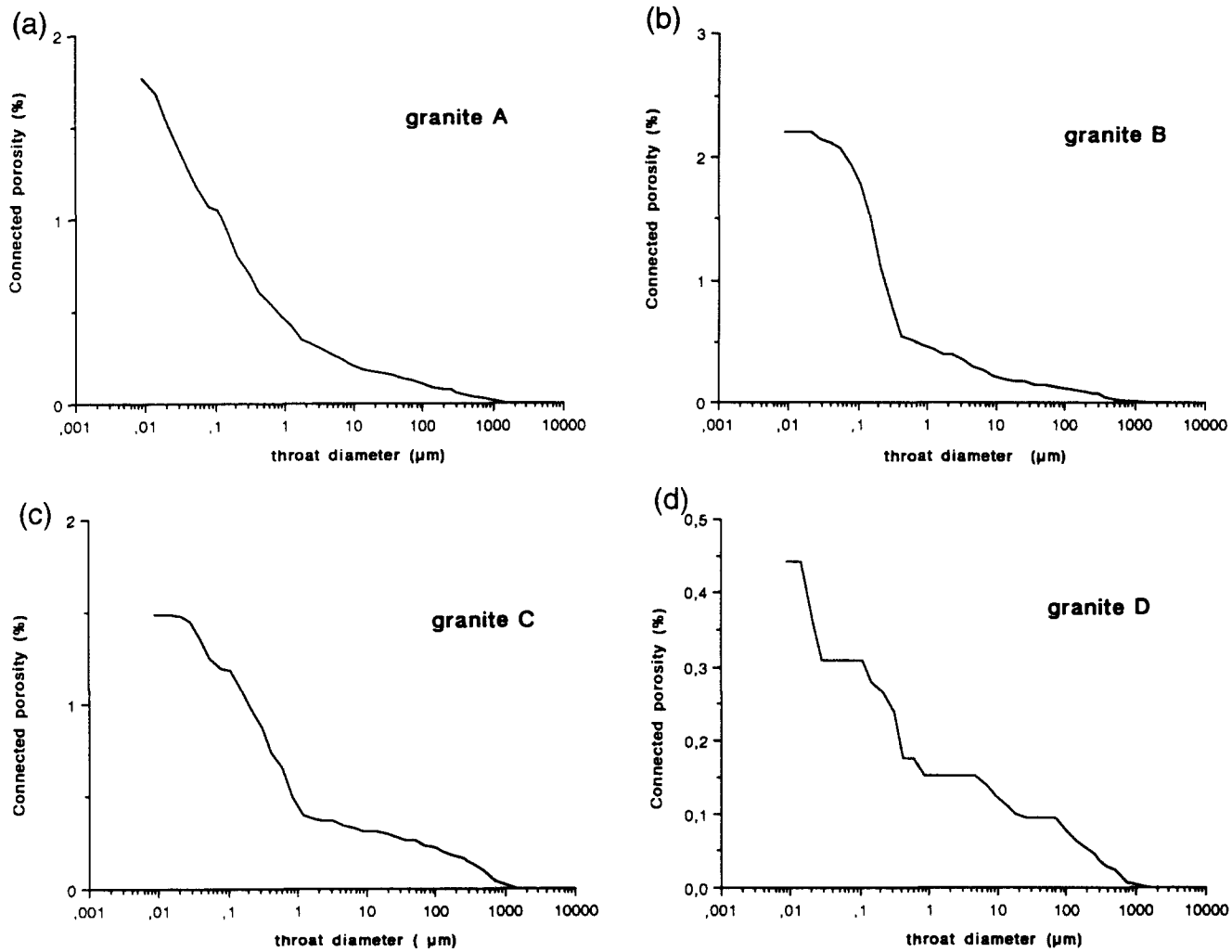

Fig. 2. Connected porosity spectra of granites A–D. (a) Granite A is a high porosity material (1.7% porosity) with throat diameter less than 1 μm. (b) Granite B has high porosity (2.3%) with throat diameter less than 0.3 μm. (c) Granite C is high porosity rock, with throat diameter <1 μm. (d) Granite D is low porosity (0.4%) with an undetermined throat diameter.

Granite A is a coarse-grained material with high connected porosity (1.77%). The value of trapped porosity indicates a high pore/crack volume ratio. This material includes widely open cracks with a low aspect ratio coefficient of 10^{-3}–10^{-5} (Figs. 2a and 3a) which are transgranular discontinuities. This granite defines a structure of low weathering material.

Granite B is a fine-grained aplitic material with high connected porosity linked to pores and a few widely open cracks (Figs. 2b and 3b). This granite has a high degree of weathering.

Granite C is medium-grained with high connected porosity due to cracks with a low shape coefficient (10^{-3}–10^{-5}); the cracks are intergranular discontinuities and their shapes are more tortuous than in A (Figs. 2c and 3c).

Granite D is coarse-grained with low connected porosity. It includes a small number of cracks with low aspect ratio. The high level of trapped porosity results from numerous pores in plagioclases feldspars which form part of the connected network (Figs. 2d and 3d).

RESULTS

Mercury injection porosity

Values of normalized connected porosity are plotted in Fig. 4. We define here the normalized connected porosity (NCP) as the connected porosity of the sample at a given temperature divided by the initial room temperature connected porosity. At low temperature, connected porosity decreases; the minimal porosity is reached at 100°C for granites B and D, and at 200°C for granites A

Fig. 3. SEM photographs of the granite samples. (a) Granite A: open cracks with low aspect ratio and alteration pores comprise the connected porosity. Cracks are transgranular structures, and weathering pores exist in potassic feldspars. (b) Granite B: connected porosity consists of interconnected pore structure. Pores are intergranular and intragranular in feldspar. (c) Granite D, a low crack density material shows that alteration pores are common in plagioclase feldspar. (d) Granite C, a high crack density material shows that cracks are intergranular and comprise an interconnected structure. Pore porosity is low. (e)–(f) explain the crack formation. (e) Grain boundaries between biotite (B) and other minerals, in granite A, are opened at 50°C. This is a disjointed boundary. (f) In granite C, a substantial proportion of grain boundaries are opened, particularly between quartz grains. (g) Granite D, at 700°C, shows that intragranular and intergranular cracks are well developed.

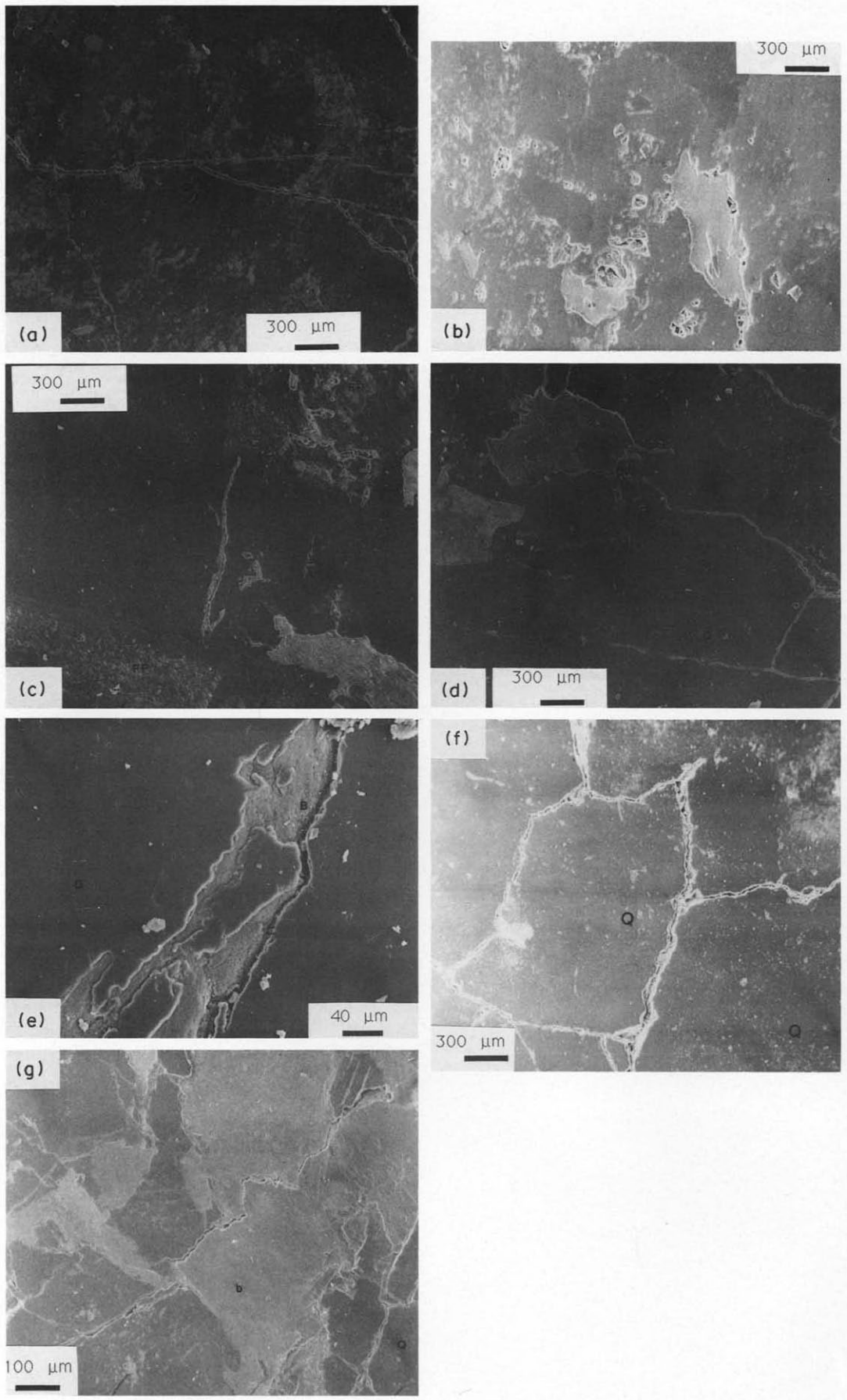

Fig. 3.

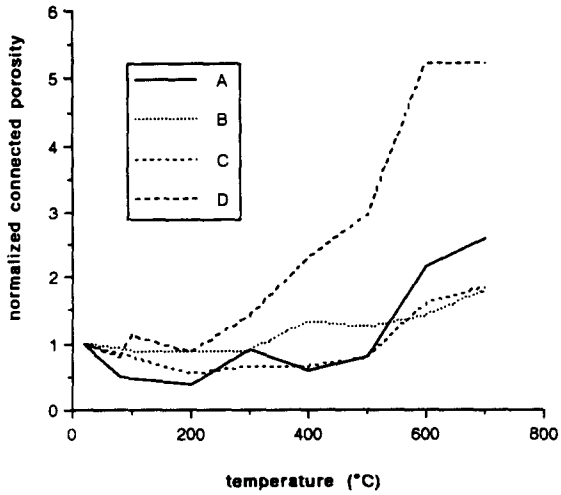

Fig. 4. Connected porosity variation for granites A, B, C and D.

and C. These temperature values allow us to determine the microcracking threshold, the temperature at which connected porosity begins to increase (Perami 1971). Two results emerge.

(1) The NCP decrease varies with initial porosity and aperture type, and is less marked for samples with high initial crack porosity rather than pore porosity (Table 2 and Fig. 4). The higher the initial crack porosity, the greater the rise in temperature required to reach a minimum porosity value.

(2) Porosity increases up to the highest experimental temperatures. Samples of granites A and C heated to a temperature of less than 500°C have a connected porosity value smaller than the non-treated sample. The connected porosity values of the samples of granites B and D heated to 400 and 300°C, respectively, are higher than the untreated sample. Between 500 and 600°C, connected porosity values increases dramatically. This is caused by the anisotropic expansion due to the quartz transition α/β which occurs at 573°C and room pressure.

The porosity spectra also evolve in two stages (Fig. 5).

(1) Up to the microcracking threshold temperature (50–200°C), granites with high crack porosity (A and C) show an important modification of the spectra (with the disappearance of large values of throat diameter), while those with low crack porosity show only a slight change in spectra.

(2) Above the microcrack threshold temperature the porosity increases by the formation of discontinuities of small throat diameter and then by enlargement of apertures and pore volume increase.

In the first stage, the low throat diameter porosity decreases (less than 1 μm for granites A, C and D and between 0.3 and 3.0 μm for granite B).

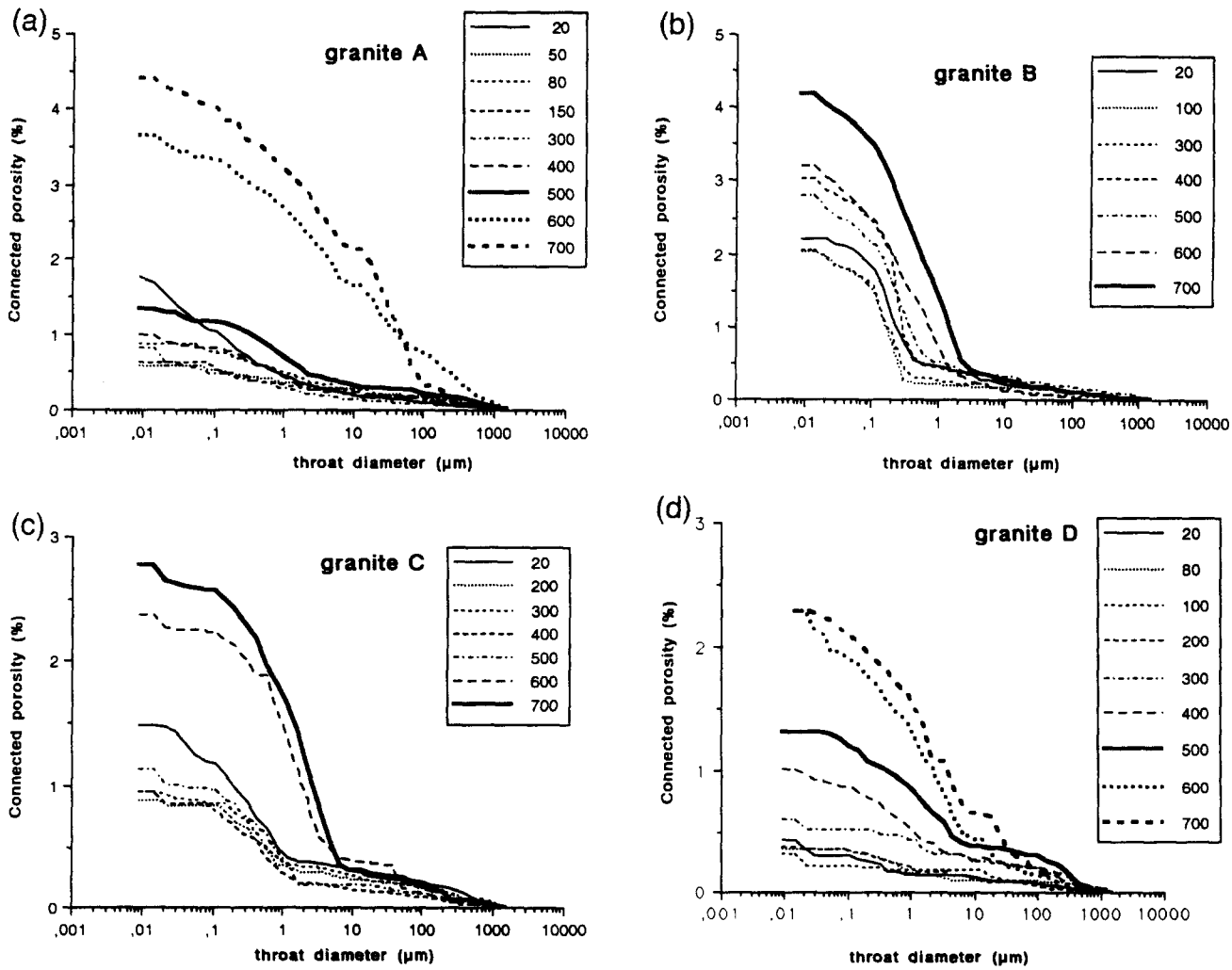

Fig. 5. Connected porosity spectra of heated samples. (a) Granite A. (b) Granite B. (c) Granite C. (d) Granite D.

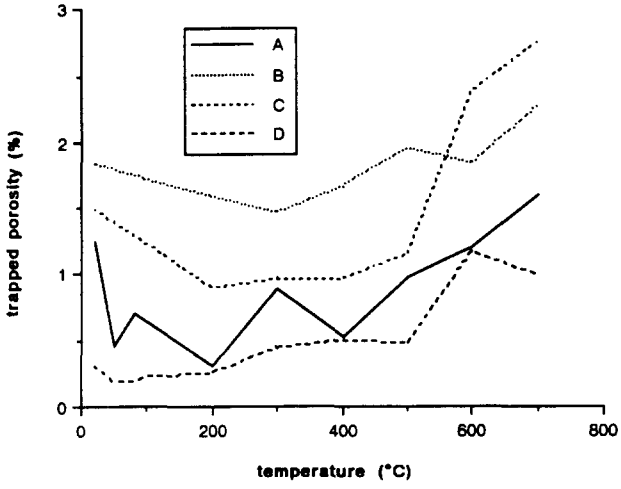

Fig. 6. Trapped porosity evolution of granites A, B, C and D.

In the second stage, up to 500°C, the connected porosity increase involves pores with a diameter of less than 1.0 μm for granites A, B and C, and less than 10 μm for granite D.

Above 600°C, the curves are shifted towards high values of porosity and throat diameter. The strong porosity increase was induced by the quartz α/β transition at 573°C (Skinner 1966). In the case of granite B, there is no evidence of this phase transition between 500 and 600°C. The grain size is probably too small to induce a significant opening of cracks. The trapped porosity evolves in two stages in a manner similar to the connected porosity (Fig. 6). In the first stage, connected porosity values decrease, with the lowest values obtained at a temperature between 50 and 300°C. Then in the second stage, the values increase for all samples systematically with temperature.

SEM observations

Two types of observations were made: qualitative observations, on each sample, and semi-quantitative measurements on samples of granites A, B and D, untreated and heated to 500 and 700°C.

Qualitative observations. Observations were made at each different temperature. *For low temperatures* (below microcracking threshold), no modifications of the initial structures, pores or cracks revealed by mercury injection porosimetry were observed. Grain boundaries between biotite and other minerals (especially quartz) in samples A and D began to open at 50°C (Fig. 3e).

For high temperatures (above microcracking threshold), up to 400°C mainly intergranular cracks formed (Fig. 3f), and at higher temperatures, both intra- and intergranular cracks formed (Fig. 3g) and the weathered regions were cracked.

Semi-quantitative measurements. The counting done on images of samples heated to various temperatures show that the higher the temperature, the more numerous and open the cracks appear to be, whereas the pore structure is not affected, and there is no diameter change or density increase (Table 3).

X-ray computerized tomography

Taking into account the set of 11 sections for each sample after each heating–cooling cycle, the total poro-

Table 3. Semi-quantitative data from the SEM analyses. The voids were counted and classified in terms of their smallest dimension (size μm) and type (pores and cracks). The average for each class was divided by the total number of voids

Granite	size (μm)	0.5	1	5	10	
A (20°C)	pore (%)	2.3	39.5	2.4	3.2	—
	crack (%)	12	10.4	7.5	4.5	—
	total/115 values	14.3	49.9	31.5	4.5	—
A (500°C)	pore (%)	2.9	34	16.6	4.3	—
	crack (%)	21	11.6	7.9	1.4	—
	total/38 values	23.9	35.6	24.5	5.7	—
A (700°C)	pore (%)	1.7	29.2	16.9	2.3	—
	crack (%)	18.1	12.3	14	4	1.2
	total/171 values	19.8	41.5	30.9	6.3	1.2
B (20°C)	pore (%)	12.2	23.3	25.5	5.5	3.3
	crack (%)	17.7	12.2	—	—	—
	total/90 values	29.9	25.5	25.5	5.5	3.3
B (500°C)	pore (%)	12	23.1	24	0.9	3
	crack (%)	19	12	3.7	1.9	—
	total/108 values	31	25.1	27.7	2.8	3
B (700°C)	pore (%)	14.3	19	17.7	5.4	—
	crack (%)	20.4	10.9	11.6	2.7	—
	total/108 values	34.7	29.9	29.3	8.1	—
D (20°C)	pore (%)	3	10.6	17.2	3.5	—
	crack (%)	30.2	17.1	13	5.4	—
	total/138 values	33.2	27.7	30.2	8.9	—
D (500°C)	pore (%)	9.2	6.7	11	3	—
	crack	25.1	25.1	12.9	6.1	0.6
	total/138 values	34.3	31.8	33.9	9.1	0.6
D (700°C)	pore (%)	10	11.9	12.6	2.5	—
	crack (%)	20.7	18.9	18.2	3.2	1.9
	total/138 values	30.7	30.8	30.8	5.7	1.9

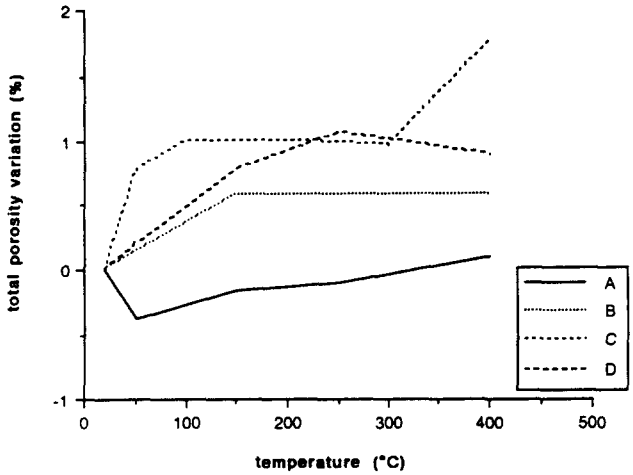

Fig. 7. Overall porosity variation of granites A, B, C and D.

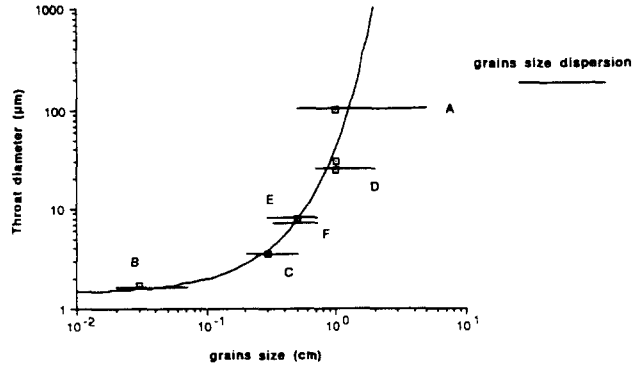

Fig. 8. Throat size–grain size relationship. The throat sizes are plotted vs the grain sizes of the different granites. The throat sizes were measured on the sample heated at 700°C: the values are the highest characteristic size of the porosity spectra. An exponential relationship is found. The E and F values are the values obtained from the Redenat and Plan de la Tour granites by Géraud & Gaviglio (1990).

sity evolution can be calculated, and is plotted in Fig. 7 for maximum temperature between 20 and 400°C.

There are two different porosity trends. In granite A, the total porosity decreases between 20 and 50°C and then increases linearly between 50 and 400°C. In granites B, C and D the total porosity increases quickly from 20°C before reaching a plateau value.

COMPARISON BETWEEN TOTAL POROSITY AND CONNECTED POROSITY

The selected granites have different structural characteristics. We have distinguished the low connected porosity material (D), the high connected porosity material (A, B and C), the low crack porosity material (B and D) and the high crack porosity material (A and C). The grain sizes decrease from granites A, D, C to B (Table 2).

Using the mercury injection porosimetry results on connected porosity and those by CT and SEM observations on both connected and unconnected porosities, two stages of porosity evolution in granite can be distinguished: below and above the microcracking threshold.

Below the microcracking threshold, between 50 and 100°C for granites B and D (low crack porosity), and 200°C for granites A and C (high crack porosity), respectively, the decrease in connected porosity concerns pore diameters less than 1.0 μm for A, C and D (Figs. 2 a–c), and between 0.3 and 3.0 μm for B (Fig. 3). These values agree with the crack width values measured on the SEM pictures of untreated samples (Table 3).

The mercury injection measurements show that the decrease in connected porosity concerns the cracks and the voids made available. However, SEM observations did not enable us to recognize or measure the modifications in structure deduced from porosity measurements. The movements involved were probably too small and too localized along the cracks to be recognized or measured on the images of heated samples.

During this first stage total porosity increased in all samples except granite A (Fig. 7). The increase in total porosity could result from the formation of new cracks : from 50°C the SEM images of samples show that many biotite grain boundaries had opened (Fig. 3e) and quartz grain boundaries were cracked (Fig. 3f). The porosity which appears unconnected in the SEM pictures could not be measured by mercury porosimetry, whereas the overall porosity of granite A decreases. It could be induced by crack closing. The particular crack morphology of this material (very linear with low aspect ratio) would seem to be responsible for the decrease in this porosity value. The opening boundaries and cracking observed for other materials are observed too on SEM pictures of granite A, but the crack formation at low temperature was not enough to counter the porosity decrease due to crack closing.

This phenomenon could be explained by the model developed by Gavrilienko & Gueguen (1989) where it appears that the crack closure depends on the elastic constants and on the cracks roughness. Their results indicate that rough cracks do not completely close even under high pressure. If we replace the hydrostatic pressure applied by these authors by the thermal pressure induced by heating assuming the sample boundaries are held fixed, the connected porosity (all granites) and overall porosity (granite A) decreases could be explained. For granite A, the relative smoothness of the cracks allows the cracks to close and the total and connected porosity decreases. For the three other materials, rough cracks, particularly in granite C, rapidly halted crack closure and induce no variation of the total porosity, but they induced a threshold closure and a decrease of the connected porosity. This result indicates the importance of the cracks on the thermal evolution of granite between 20°C and the microcracking threshold. Initial cracks induce a decrease of connected porosity by threshold closing and, for particular crack morphology, a total porosity decrease.

Above the microcracking threshold, connected and total porosities increase. The connected porosity increase is less than the total value. This fact shows that the total porosity is created before it is incorporated into the connected network, so that the connected porosity is

composed of formly isolated cracks (from the preceding stage) now connected, as shown by SEM pictures.

Semi-quantitative SEM data corroborate the large opening of cracks between 500 and 700°C induced by the α/β quartz transition. Pore discontinuities are not affected by the thermal porosity which is induced by the development of the crack network shown on the SEM pictures.

The values of the largest throat diameters measured after heating to 700°C are plotted vs the grain size (Table 2) in Fig. 8; data obtained for two other granites (Géraud & Gaviglio 1990) are also plotted. There is a relationship between these two parameters for the highest temperature. But there is no relationship between the grain size and the normalized connected porosity: the porosity value for granite B (with the smallest grain size) is higher than for granite C. The grain size, for high temperature crack opening is an important factor for the permeability calculation (see above). Thus, the grain size is an important parameter for the permeability evolution during thermal cycling.

CONCLUSIONS

Measurements of different characteristics of residual porosity in several granites, combined with SEM observation of polished surfaces in samples deformed at different temperatures, demonstrate that the granite structure is modified in two stages.

(1) A phase of decreasing opening porosity is dependent on fracture porosity. This occurs at low temperatures (<200°C). For the same temperature range the overall porosity increases due to the formation of cracks.

(2) A phase of increase in opening porosity is due to the connection of networks of discontinuities created during the previous phase, and to an increase in number and cracks opening.

Porosity is influenced by initial porosity for deformations at low temperatures. For intermediate temperatures (300–500°C) initial porosity and grain size are the main controlling factors. At high temperatures the main factor is grain size. Indeed aperture size is controlled by grain size. At lower temperatures there is also the influence of the value and type of initial porosity.

Although at maximum temperatures the induced porosity value cannot be directly linked to textural or structural parameters, the maximum throat size value can be related to grain size. At lower temperatures, the porosity and aperture values depend on two main parameters: grain size and initial porosity.

The values of connected and total porosity explain changes in permeability and mechanical characteristics given by numerous authors. Thus it is necessary to measure both types of porosity to obtain an accurate idea of the evolution of a rock undergoing a heating cycle.

Acknowledgements—We would like to thank D. Mainprice for his thoughtful discussions and review, and the two reviewers for corrections and suggestions.

REFERENCES

Cooper, H. W. & Simmons, G. 1977. The effect of cracks on the thermal expansion of rocks. *Earth Planet. Sci. Lett.* **36**, 404–412.

Friedman, M. & Johnson, B. 1978. Thermal cracking in unconfined Sioux quartzite. *Proc. 19th U.S. Symp. of Rocks Mech.*, Reno, 423–430.

Friedrich, J. & Wong, T. F. 1986. Micromechanics of thermally induced cracking in three crustal rocks. *J. geophys. Res.* **91**, 12,743–12764.

Gavrilenko, P. & Guegen, Y. 1989. Pressure dependence of permeability : a model for cracked rocks. *Geophys. J. Int.* **98**, 159–172.

Géraud, Y. & Gaviglio, P. 1990. Modifications expérimentale de la texture de granites par chauffage : évolution de la porosité et de la densité en fonction de la température. *C. r. Acad. Sci., Fr.*, Sér. II **310**, 1681–1686.

Géraud, Y., Mazerolle, F. & Raynaud, S. 1991. Essai de quantification de la porosité d'un granite altéré, utilisation du scanner médical (tomodensitométrie X). *Journée S.G.F./I.S.S. du 8 Fevrier 1991, du compteur de point à l'analyseur d'images*, 41–44.

Guegen, Y & Diennes, J. K. 1989. Transport properties of rocks from statistics and percolation. *Math. Geol.* **21**, 1–13.

Heuze, F.E. 1983. High temperature mechanical, physical and thermal properties of granite rocks—a review. *Int. J. Rock Mech. & Mining Sci. & Geomech. Abs.* **20**, 3–10.

Katsube, T. J. & Kamineni, D. C. 1983. Effect of alteration on pore structure of crystalline rocks : core samples from Atikokan, Ontario. *Can. Mineralogist* **21**, 637–646.

Katz, A. J. & Thompson, A. H. 1987. Prediction of rock electrical conductivity from mercury injection measurements. *J. geophys. Res.* **92**, 599–607.

Krantz, R. L. 1980. Crack growth and development during creep of Barre granite. *Int. J. Rock Mech. & Mining Sci. & Geochem. Abs.* **1**, 23–35.

Krantz, R. L. 1983. Microcracks in rocks : a review. *Tectonophysics* **100**, 449–480.

Lenormand, R., Zarcone, C. & Sarr, A. 1983. Mechanisms of the displacement of one fluid by another in a network of capillary ducts. *J. Fluid. Mech.* **135**, 337–353.

Li, Y. & Wardlaw, N. C. 1986. Mechanisms of nonwetting phase trapping during imbibition at slow rates. *J. Colloid Inter. Sci.* **109**, 473–486.

Norton, D. & Knapp, R. 1977. Transport phenomena in hydrothermal systems : the nature of porosity. *Am. J. Sci.* **277**, 913–936.

Norton, D. & Knight, 1977. Transport phenomena in hydrothermal systems : cooling plutons. *Am. J. Sci.* **277**, 937–981.

Perami, R. 1971. Formation des microfissures dans les roches sous l'effet de variations homogènes de témperature. *Symp. Soc. Inter. Mec. Roches*, Nancy, 1–6.

Raynaud, S., Fabre, D., Mazerolle, F., Géraud, Y. & Latière, H. J. 1989. Analysis of the internal structure of rocks and characterization of mechanical deformation by non-destructive method : X-Ray tomodensitometry. *Tectonophysics* **159**, 149–159.

Skinner, B. J. 1966. Thermal expansion. In: *Handbook of Physical constants* (edited by Clark, S. P.). *Mem. geol. Soc. Am.* **97**, 75–96.

Sprunt, E. S. & Brace, W. F. 1974. Direct observation of microcavities in crystalline rocks. *Int. J. Rock Mech. & Mining & Geochem. Abs.* **11**, 139–150.

Tapponier, P. E. & Brace, W .F. 1976. Development of stress induced microcracks in Westerly granite. *Int. J. Rock Mech. & Mining Sci. & Geochem. Abs.* **13**, 103–112.

Washburn, E. W. 1921. Note on a method of determining the distribution of pore sizes in a porous material. *Proc. natn. Acad. Sci. U.S.A.* **7**, 115–116.

Wang, H. F., Bonner, B. P., Carlson, S. R., Kowallis, B. J. & Heard, H. C. 1989. Thermal stress cracking in granite. *J. geophys. Res.* **94**, 1745–1758.

Wardlaw, N. C., McKellar, M. & Li, Y. 1988. Pore and throat distributions determined by mercury injection porosimetry and direct observation. *Carbonates & Evaporites* **3**, 1–15.